Chin. J. Astron. Astrophys. Vol. 7 (2007), No. 6, 777–788
(*http://www.chjaa.org*)

Chinese Journal of
Astronomy and
Astrophysics

Very Early Optical Afterglows for Geometric Models of X-ray Flashes and X-ray Rich GRBs *

Ting Yan[1,2,3], Da-Ming Wei[1,2,4] and Yi-Zhong Fan[1,2,5]

[1] Purple Mountain Observatory, Chinese Academy of Sciences, Nanjing 210008; *tyan@pmo.ac.cn*
[2] National Astronomical Observatories, Chinese Academy of Sciences, Beijing 100012
[3] Department of Astrophysical and Planetary Sciences, University of Colorado, Boulder, CO 80309, USA
[4] Joint Center for Particle Nuclear Physics and Cosmology of Purple Mountain Observatory - Nanjing University, Nanjing 210008
[5] The Racah Institute of Physics, Hebrew University, Jerusalem 91904, Israel

Received 2007 January 19; accepted 2007 June 3

Abstract If X-ray flashes (XRFs) and X-ray rich Gamma-ray Bursts (XRRGs) have the same origin as the Gamma-ray bursts (GRBs) but are viewed off-center from structured jets, their early afterglows may differ from those of GRBs, and when the ultra-relativistic outflow interacts with the surrounding medium, there are two shocks formed, a forward shock (FS), and a reverse shock (RS). We calculate numerically the early afterglow powered by uniform jets, Gaussian jets and power-law jets in the forward-reverse shock scenario. A set of differential equations govern the dynamical evolution. The synchrotron self-Compton effect has been taken into account in the calculation. In the uniform jets, the very early afterglows of XRRGs and XRFs are significantly lower than the GRBs and the observed peak times of RS emission are later in the interstellar medium environment. The RS components in XRRGs and XRFs are difficult to detect, but in the stellar wind environment, the reduction of the very early flux and the delay of the RS peak time are not so remarkable. In nonuniform jets (Gaussian and power-law jets), where there are emission materials on the line of sight, the very early light curve resembles equivalent isotropic ejecta in general although the RS flux decay index shows notable deviations if the RS is relativistic (in stellar wind).

Key words: X-rays: general — Gamma rays: bursts — radiation mechanisms: non-thermal

1 INTRODUCTION

Late time GRB afterglow emission has been well observed and studied since the first detection in 1997 (van Paradijs et al. 1997; Costa et al. 1997). After the launch of *Swift* , the early afterglow, especially in X-ray band, has also been observed intensively. This early afterglow may provide important information about the initial parameters of the burst and shed light on the explosion mechanism. In the standard baryonic GRB fireball model, prompt GRB emission is produced by collisions of internal shocks and the afterglow comes from interactions between burst-ejected materials and the circum-burst medium. After the internal shock phase, when the fireball has been decelerated by the circumburst medium, usually a pair of shocks emerges (Mészáros & Rees 1997; Sari & Piran 1999). One is a forward shock expanding outward to heat the external medium, the other is a reverse shock (RS) propagating into the ejecta and heats the cold initial shell. Energy is gradually transferred from the center to the outer medium through the shocked medium and ejecta. The early afterglow studied in this paper is during this transition stage.

* Supported by the National Natural Science Foundation of China.

Mészáros & Rees (1997) pointed out that the RS should emit detectable optical synchrotron photons. This prediction has been confirmed by the optical flash and radio flare detected in GRB 990123 (Akerlof et al. 1999; Kulkarni et al. 1999; Sari & Piran 1999; Mészáros & Rees 1999; Nakar & Piran 2004). The later more detailed investigations suggested that the RS region may be magnetized (Fan et al. 2002; Zhang, Kobayashi & Mészáros 2003; Panaitescu & Kumar 2004). Now, the RS emission has been studied intensively from a theoretical standpoint, for instance, the RS emission in stellar wind medium (Chevalier & Li 2000; Wu et al. 2003; Koboyashi & Zhang 2003; Zou, Wu & Dai 2005); that powered by magnetized outflow or neutron-fed outflow (Fan et al. 2004b; Zhang & Kobayashi 2005; Fan et al. 2005a); and the pair-rich RS emission (Li et al. 2003a; McMahon, Kumar & Piran 2005), but on the observational side, there have only been a few additional candidates, namely, GRB 021211 (Fox et al. 2003; Li et al. 2003b; Wei 2003; Kumar & Panaitescu 2003), GRB 041219a (Blake et al. 2005; Fan et al. 2005b), GRB 050525a (Klotz et al. 2005; Shao & Dai 2005), GRB 050904 (Boër et al. 2006; Wei et al. 2006), and GRB 060111b (Klotz et al. 2006). Whether the lack of RS emission events is due to observational limitations or some theoretical problems may be settled by further observations.

XRFs are an interesting phenomenon which resembles GRBs. They are similar to GRBs in many aspects except their lower peak energies ($\sim$10 keV) and lower isotropic energies ($\sim 10^{51}$ erg). Several models have been proposed so far (Dermer, Chiang & Böttcher 1999; Heise et al. 2001; Huang, Dai & Lu 2002; Barraud et al. 2003; Lamb, Donaghy & Graziani 2005). Among them the structured jet model is widely discussed (see Zhang 2007 for a recent review). According to this model, observers at different viewing angles see different phenomena. GRBs are observed near the axis of the jet and XRFs may be detected at the edge of the jet. Between them are the XRRGs whose peak energy and isotropic energy are in between the two. Possible jet models for the XRFs and XRRGs include the off-beam uniform jet model (Ioka & Nakamura 2001; Yamazaki, Ioka & Nakamura 2002), the Gaussian jet model (Zhang & Mészáros 2002; Lloyd-Ronning, Dai & Zhang 2004; Zhang, Dai & Lloyd-Ronning 2004), and the power-law jet model (Mészáros et al. 1998; Jin & Wei 2004). The very early afterglow powered by structured jets has been calculated by Fan et al. (2004a) analytically. In this work, we present our numerically obtained results.

The dynamical evolution is described in Section 2. The radiation calculation procedure is described in Section 3. Afterglows from different jets are presented in Section 4. In section 5, our results are summarized, together with a discussion.

2 DYNAMICAL EVOLUTION

Consider a homogenous cold shell ejected from the central engine with an isotropic energy $E_{\rm iso}$ and width Δ_0. It expands relativistically with Lorenz factor η, then its mass is $m_{\rm ej} = E_{\rm iso}/\eta c^2$. When an FS and an RS are formed, there is a shocked region which consists of two parts: the shocked medium and the shocked shell, separated by the contact discontinuity surface. The shocked region is assumed to have homogenous bulk velocity and energy density, that is, $\gamma_2 = \gamma_3$, $e_2 = e_3$ (hereafter the subscript 2 denotes the shocked medium, subscript 3, the shocked shell and subscript 4, the cold ejecta). However, the number density and random particle velocity in the comoving frame are discontinuous at the contact surface. The random Lorentz factor of the shocked protons is $(\gamma_2 - 1)$ in region 2 and $(\gamma_{34} - 1)$ in region 3 (Blandford & Mckee 1976), where γ_{34} is the relative Lorentz factor of the shocked shell to the cold shell.

The kinetic energies of the shocked medium, the shocked shell and the unshocked shell are respectively:

$$\begin{aligned} E_2 &= (\gamma_2 - 1)m_2c^2 + (1 - \epsilon_2)\gamma_2 U_2, \\ E_3 &= (\gamma_3 - 1)m_3c^2 + (1 - \epsilon_3)\gamma_3 U_3, \\ E_4 &= (\eta - 1)(m_{\rm ej} - m_3)c^2, \end{aligned}$$

where $U_2 = (\gamma_2 - 1)m_2c^2$ and $U_3 = (\gamma_{34} - 1)m_3c^2$. U_2 and U_3 are the internal energies in the comoving frame. If a fraction ϵ of the energy in the fresh shocked material is radiated, the radiated thermal energies of the shocked medium and the shocked shell are $\epsilon_2\gamma_2(\gamma_2 - 1){\rm d}m_2c^2$ and $\epsilon_3\gamma_3(\gamma_{34} - 1){\rm d}m_3c^2$, respectively. With energy conservation, we have

$$\begin{aligned} {\rm d}(E_2 + E_3 + E_4) = &-\epsilon_2\gamma_2(\gamma_2 - 1){\rm d}m_2c^2 \\ &-\epsilon_3\gamma_3(\gamma_{34} - 1){\rm d}m_3c^2 \,. \end{aligned} \quad (1)$$

If GRBs are located in the interstellar medium (ISM), the number density of the external medium n_1 is constant. If GRBs are born in stellar winds, then $n_1 = AR^{-2}$, where $A = \dot{M}/4\pi m_{\rm p} v_{\rm w} = 3\times10^{35} A_* \ {\rm cm}^{-1}$ and $A_* = (\dot{M}/1\times10^{-5}{\rm M}_\odot \ {\rm yr}^{-1})(v_{\rm w}/10^3 \ {\rm km \ s}^{-1})^{-1}$ (Dai & Lu 1998; Chevalier & Li 2000). The swept-up mass of FS evolves as

$$\frac{{\rm d}m_2}{{\rm d}R} = 4\pi R^2 n_1 m_{\rm p} \, . \tag{2}$$

The comoving number density of the ejecta $n_4 = m_{\rm ej}/4\pi m_{\rm p} R^2 \Delta\eta$, where $\Delta = \max(\Delta_0, R/\eta^2)$, which is the width of shell after allowing for spreading. The spreading radius $R_{\rm s} = \Delta_0\eta^2$. When R is smaller than $R_{\rm s}$, $\Delta \approx \Delta_0$. If $R > R_{\rm s}$, $\Delta \approx R/\eta^2 > \Delta_0$. The swept-up mass of RS evolves as

$$\frac{{\rm d}m_3}{{\rm d}R} = 4\pi R^2 (\beta_4 - \beta_{\rm RS}) \eta \, n_4 m_{\rm p} \, , \tag{3}$$

where $\beta_{\rm RS} = \frac{\gamma_3 n_3 \beta_3 - \gamma_4 n_4 \beta_4}{\gamma_3 n_3 - \gamma_4 n_4}$, which is the Lorentz factor of the RS (Fan et al. 2004b). From Equations (1)–(3), it is found that γ_2 evolves as

$$\frac{{\rm d}\gamma_2}{{\rm d}R} = -4\pi R^2 \frac{Q}{P}, \tag{4}$$

where

$$\begin{aligned} Q &= (\gamma_2^2 - 1) n_1 m_{\rm p} + (\gamma_2\gamma_{34} - \eta)(\eta n_4 m_{\rm p})(\beta_4 - \beta_{\rm RS}), \\ P &= m_2 + m_3 + (1-\epsilon_2)(2\gamma_2 - 1) m_2 + (1-\epsilon_3)(\gamma_{34} - 1) m_3 \\ &\quad + (1-\epsilon_3)\gamma_2 m_3 [\eta(1 - \beta_2\beta_4) - \frac{\eta\beta_4}{\gamma_2^2\beta_2}]. \end{aligned}$$

The overall dynamical evolution of RS-FS can be obtained by solving Equations (2)–(4) combined with

$${\rm d}R = \frac{\beta_2}{1-\beta_2} \frac{c{\rm d}t}{1+z} \, , \tag{5}$$

where t is the time measured by the observer and z is the redshift.

Let $\eta_{\rm e}$ denote the electron radiative efficiency, that is, a fraction $\eta_{\rm e}$ of the electron energy is radiated. In the fast cooling stage, electrons cool immediately and $\eta_{\rm e} = 1$. In the slow cooling stage, $\eta_{\rm e} = (\gamma_{\rm m}/\gamma_{\rm c})^{p-2}$ (Sari & Esin 2001), where $\gamma_{\rm m}$ is the minimum Lorentz factor and $\gamma_{\rm c}$ is the cooling Lorentz factor of the shocked electrons (see detail in the next section). Usually it is assumed that electrons share a fraction $\epsilon_{\rm e}$ of the internal energy, then the radiative efficiency is

$$\epsilon = \epsilon_{\rm e}\eta_{\rm e} = \epsilon_{\rm e} \min[1, (\gamma_{\rm m}/\gamma_{\rm c})^{p-2}], \tag{6}$$

with $\epsilon = 0$ for the adiabatic case and $\epsilon = 1$ for the fully radiative case.

Sari & Piran (1995) introduced $\xi \equiv (l/\Delta_0)^{1/2}\eta^{-4/3}$ to describe the strength of the RS, where l is the Sedov length. At the RS crossing time ($t_\times$), if $\xi < 1$, the RS is relativistic (RRS). If $\xi > 1$ at $t_\times$, the RS is non-relativistic (NRS). In the stellar wind case, Wu et al. (2003) found a similar parameter $\zeta \equiv (l/\Delta_0)^{1/2}\eta^{-2}$ to determine the strength of RS. Our results are consistent with theirs. The scaling laws are exactly the same as the analytical results though differences exist in the absolute values. In our numerical results, it is found out that $\gamma_{34} - 1$ can be well fitted by

$$\begin{aligned} \lg(\gamma_{34} - 1) &= -0.64991 - 1.64406 \lg\xi \\ &\quad -0.59494(\lg\xi)^2 - 0.13656(\lg\xi)^3, \end{aligned} \tag{7}$$

$$\begin{aligned} \lg(\gamma_{34} - 1) &= -0.88759 - 1.20563 \lg\zeta \\ &\quad -0.28507(\lg\zeta)^2 - 0.04115(\lg\zeta)^3, \end{aligned} \tag{8}$$

for $0.01 < \xi(\zeta) < 10$ (Fig. 1).

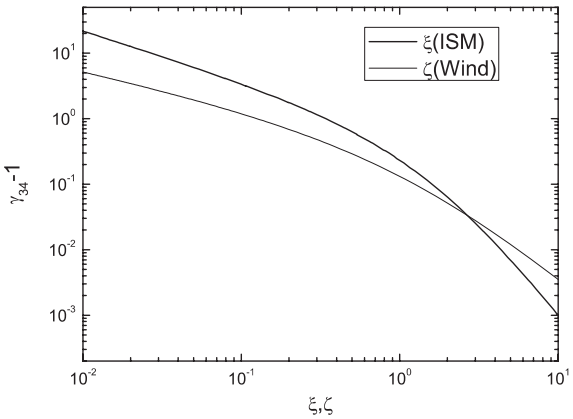

Fig. 1 Strength of the reverse shock at the reverse shock crossing time. Here γ_{34} is the relative Lorentz factor of the shocked shell to the cold shell, ξ and ζ are dependent on the initial parameters of the ejecta (see Sect. 2 for details).

After the RS crosses the shell, the shocked medium and the shocked ejecta evolve somewhat independently. The FS continues to spread outwards, collects external medium, and the shocked medium is gradually shaped into BM self-similar profile. Energy conservation still applies:

$$\mathrm{d}E_2 = -\epsilon_2\gamma_2(\gamma_2 - 1)m_2c^2\,, \qquad (t > t_\times)\,. \tag{9}$$

Then the forward shock evolution can be solved together with Equations (2), (5) and (9). At the same time, the shocked ejecta cease to increase, i.e., $m_3 = m_{\rm ej} = \mathrm{const.}$ for $t > t_\times$. Koboyashi & Sari (2000) showed that its evolution is approximately consistent with the BM solution, that is, $\gamma_3 \propto R^{-7/2+k}$ ($k = 0$ applies to ISM and $k = 2$ to wind). They also inferred that the shocked ejecta spread with the speed of light in the comoving frame and evolve adiabatically.

3 RADIATION

Both the FS and RS heat the cold materials to higher temperatures, accelerate the protons and electrons as well as generate a random magnetic field. Here we calculate the synchrotron radiation and the synchrotron self-Compton cooling of the shocked electrons. The internal energy density of the FS shocked medium is $e_2 = 4\gamma_2^2 n_1 m_{\rm p}c^2$ (Blandford & Mckee 1976). For the ejecta shocked by the RS, $e_3 = e_2$ before $t_\times$, otherwise $e_3 \propto t^{-\frac{4(3+g)}{3(1+2g)}}$ ($g = 7/2 - k$), here $\epsilon_{\rm e}$ and $\epsilon_{\rm B}$ are defined to be the fraction of internal energy belonging to the electrons and magnetic field. It is easy to obtain the magnetic field $B = \sqrt{8\pi\epsilon_{\rm B}e}$. As to the electrons, in the absence of energy loss, they are assumed to be shocked to a power-law distribution, $\mathrm{d}N_{\rm e}/\mathrm{d}\gamma_{\rm e} \propto \gamma_{\rm e}^{-p}(\gamma_{\rm m} < \gamma_{\rm e} < \gamma_{\rm M}, p > 2)$, with the minimum Lorentz factor

$$\gamma_{\rm m,2} = \epsilon_{\rm e}(\gamma_2 - 1)\frac{m_{\rm p}(p-2)}{m_{\rm e}(p-1)} + 1,$$

$$\gamma_{\rm m,3} = \epsilon_{\rm e}(\gamma_{34} - 1)\frac{m_{\rm p}(p-2)}{m_{\rm e}(p-1)} + 1,$$

and maximum Lorentz factor $\gamma_{\rm M} = 10^8(B/1\mathrm{G})^{-1/2}$ (Wang, Dai & Lu 2001). Here e and B are all measured in the comoving frame. Following Sari et al. (1998), we introduce the cooling Lorentz factor $\gamma_{\rm c} = \frac{6\pi(1+z)m_{\rm e}c}{\sigma_{\rm T}\gamma B^2 t}$ to describe the synchrotron radiation loss of the shocked electrons. Note that $\gamma_{\rm c,3} = \gamma_{\rm c,2}$ before $t_\times$. The actual electron distribution should be given as following (see also Fan et al. 2004b): (i) For $\gamma_{\rm c} \le \gamma_{\rm m}$, i.e., the fast cooling case,

$$\frac{\mathrm{d}N_{\rm e}}{\mathrm{d}\gamma_{\rm e}} = C_1 \begin{cases} \gamma_{\rm e}^{-2}\,, & (\gamma_{\rm c} \le \gamma_{\rm e} \le \gamma_{\rm m}), \\ \gamma_{\rm m}^{p-1}\gamma_{\rm e}^{-(p+1)}\,, & (\gamma_{\rm m} < \gamma_{\rm e} \le \gamma_{\rm M}), \end{cases} \tag{10}$$

where

$$C_1 = \Big[\frac{1}{\gamma_{\rm c}} - \frac{p-1}{p}\frac{1}{\gamma_{\rm m}} - \frac{\gamma_{\rm m}^{p-1}\gamma_{\rm M}^{-p}}{p}\Big]^{-1} N_{\rm tot}\,,$$

$N_{\rm tot}$ is the total number of radiating electrons involved; (ii) For $\gamma_{\rm m} < \gamma_{\rm c} \leq \gamma_{\rm M}$, i.e., the slow cooling case

$$\frac{{\rm d}N'_{\rm e}}{{\rm d}\gamma_{\rm e}} = C_2 \begin{cases} \gamma_{\rm e}^{-p}\,, & (\gamma_{\rm m} \leq \gamma_{\rm e} \leq \gamma_{\rm c}), \\ \gamma_{\rm c}\gamma_{\rm e}^{-(p+1)}\,, & (\gamma_{\rm c} < \gamma_{\rm e} \leq \gamma_{\rm M}), \end{cases} \tag{11}$$

where

$$C_2 = [\frac{\gamma_{\rm m}^{1-p}}{p-1} - \frac{\gamma_{\rm c}^{1-p}}{p(p-1)} - \frac{\gamma_{\rm c}\gamma_{\rm M}^{-p}}{p}]^{-1} N_{\rm tot}.$$

In the comoving frame, the synchrotron radiation of the two-segment distribution of electrons can be well described by a power-law spectrum consistingg of several segments. The spectrum peaks at $\min(\nu'_{\rm m}, \nu'_{\rm c})$ with flux (Wijers & Galama 1999)

$$F'_{\rm max} = \Phi_{\rm p}\frac{\sqrt{3}e^3 B N_{\rm tot}}{m_{\rm e}c^2}, \tag{12}$$

where $\Phi_{\rm p}$ is a function of p (for $p \simeq 2.5, \Phi_{\rm p} \simeq 0.60$). The break frequencies corresponding to $\gamma_{\rm m}$ and $\gamma_{\rm c}$ are $\nu'_{\rm m} = 3\gamma_{\rm m}^2 eB/(4\pi m_{\rm e}c)$ and $\nu'_{\rm c} = 3\gamma_{\rm c}^2 eB/(4\pi m_{\rm e}c)$. The absorption frequency $\nu'_{\rm a}$, below which the synchrotron self-absorption cannot be ignored, is calculated according to Wu et al. (2003). These three break frequencies divide the spectrum into four segments. The spectrum indices are, for increasing frequencies,

(i) for $\nu'_{\rm a} < \nu'_{\rm m} < \nu'_{\rm c}$, $[2, 1/3, (1-p)/2, -p/2]$;
(ii) for $\nu'_{\rm a} < \nu'_{\rm c} < \nu'_{\rm m}$, $[2, 1/3, -1/2, -p/2]$;
(iii) for $\nu'_{\rm m} < \nu'_{\rm a} < \nu'_{\rm c}$, $[2, 5/2, (1-p)/2, -p/2]$;
(iv) for $\nu'_{\rm c} < \nu'_{\rm a} < \nu'_{\rm m}$, $[2, 5/2, -1/2, -p/2]$;
(v) for $\nu'_{\rm m} < \nu'_{\rm c} < \nu'_{\rm a}$ and $\nu'_{\rm c} < \nu'_{\rm m} < \nu'_{\rm a}$, $[2, 5/2, 5/2, -p/2]$.

We assume that the synchrotron power is radiated isotropically in the comoving frame, $\frac{{\rm d}F'(\nu')}{{\rm d}\Omega'} = \frac{F'(\nu')}{4\pi}$. The angular distribution of power in the observer's frame is (Rybicki & Lightman 1976; Huang et al. 2000)

$$\frac{{\rm d}F(\nu)}{{\rm d}\Omega} = \frac{1+z}{\gamma^3(1-\beta\mu)^3}\frac{{\rm d}F'(\nu')}{{\rm d}\Omega'} = \frac{1+z}{\gamma^3(1-\beta\mu)^3}\frac{F'(\nu')}{4\pi}, \tag{13}$$

where $\nu = \frac{\nu'}{(1+z)\gamma(1-\mu\beta)}$ and $\mu = \cos\Theta$, Θ is the angle between the radiation region and the viewing line in the burst frame. Then the observed flux density at frequency ν is

$$\begin{aligned} S_\nu &= \frac{1}{A}\left(\frac{dF(\nu)}{d\Omega}\frac{A}{D_{\rm L}^2}\right) \\ &= \frac{1+z}{\gamma^3(1-\beta\mu)^3}\frac{1}{4\pi D_{\rm L}^2}F'\left((1+z)\gamma(1-\mu\beta)\nu\right), \end{aligned} \tag{14}$$

where A is the area of our detector and $D_{\rm L}$ the luminosity distance (we assume $H_0 = 65\ {\rm km\ s^{-1}\ Mpc^{-1}}$, $\Omega_{\rm M} = 0.3$ and $\Omega_\wedge = 0.7$).

After the RS crosses the shell, no new electrons are accelerated in the shocked shell and all the electrons cool at the same rate by the adiabatic expansion of the fluid. No electrons exist above $\gamma_{\rm c}$, so the flux above $\nu'_{\rm c}$ drops exponentially.

At any given time t, the photons received by the observer come from an equal arriving time surface determined by (Huang et al. 2000)

$$t = (1+z)\int\frac{1-\beta\cos\Theta}{\beta c}{\rm d}R \equiv \text{const.} \tag{15}$$

We also consider synchrotron self-Compton (SSC) effect. It will reduce the cooling Lorentz factor to

$$\gamma_{\rm c} = \frac{\gamma_{\rm c}^{\rm syn}}{1+Y}\,, \tag{16}$$

where Y is the Compton parameter, expressed as (Wei & Lu 1998; Sari & Esin 2001; Wang, Dai & Lu 2001)

$$Y = \frac{L_{\rm ICS}}{L_{\rm syn}} = \frac{\eta_{\rm e}\epsilon_{\rm e}/\epsilon_{\rm B}}{1+Y} = \frac{-1+\sqrt{1+4\eta_{\rm e}\epsilon_{\rm e}/\epsilon_{\rm B}}}{2}. \quad (17)$$

Insert this in Equation (16), and $\gamma_{\rm c}$ can be solved numerically. At the early time, the forward shocked material is in the fast cooling phase and the cooling frequency will be reduced significantly due to the SSC radiation. As to the RS, whether it is in the fast or slow cooling phase depends on the parameters. However, even if it is in the slow cooling phase, the cooling frequency will be suppressed by SSC if $\epsilon_{\rm e}/\epsilon_{\rm B} \gg 1$, which is usually the case.

4 NUMERICAL RESULTS

In this section we first present the early afterglow from the isotropic ejecta. We then calculate the afterglows powered by different types of jets. Three types are considered: the uniform jet, the Gaussian jet, and the power-law jet. Sideways expansion of the jet is ignored in our calculation.

The obstacle we encountered in the current work is the poorly known initial Lorentz factor of the jets, especially for the structured ones (the Gaussian jet and power-law jet). By now, the spectra of most XRFs are non-thermal. The emitting region should be optically thin, i.e., the optical thickness $\tau = n_{\rm e}\sigma_{\rm T}R' < 1$, where R' is the comoving width of the emitting region, $n_{\rm e} \approx \frac{L}{16\pi\epsilon_{\rm e}\eta^5 m_{\rm p}c^4\delta t R'}$ is the comoving number density of electrons contained in the emitting region, L the isotropic luminosity of the burst, and δt the typical variability timescale of the burst lightcurve. Assuming that the XRFs are powered by internal shocks, the optical thin ($\tau < 1$) condition yields (e.g., Fan & Wei 2005)

$$\eta \geq 30 L_{49}^{1/5}\delta t_{-2}^{-1/5}. \quad (18)$$

Kumar & Granot (2003) have made a numerical investigation on the hydrodynamical evolution of a Gaussian jet by assuming $\eta(\theta)$ is also Gaussian. In the Monte Carlo simulation of Zhang et al. (2004), $\eta(\theta)$ was taken as a free function but it was found that a flat or only small fluctuation angular distribution of Lorentz factor is actually required. Therefore, and partly for convenience, we take $\eta = 300$ for an off-axis uniform jet, the Gaussian jet, and the power-law jet. As a test of this assumption, we estimate the initial Lorentz factor of XRF 050406 (Romano et al. 2006) and 050416A (Mangano et al. 2007). Following Zhang et al. (2006), with the given kinetic energy of the outflow and the earliest X-ray power-law decay time (excluding the very early sharp drop), we have $\Gamma \geq 100$. Our assumption is thus reasonable.

For each jet model, light curves with typical parameters from three viewing angles are presented, which may respectively correspond to the GRBs, XRRGs and XRFs. The light curves differ from each other although there are some properties in common. Viewing from the center of a jet, the light curve is approximately the same as that powered by isotropic ejecta at the early time and a break occurs when the emission from the edge comes into view. When we observe off-axis, the flux is lower at the early time but gradually converges to the light curve from the center when the whole jet can be seen.

4.1 Isotropic Ejecta

The upper panel of Figure 2 shows the early R band light curve from isotropic ejecta in the ISM case with typical parameters. The RS dominates the very early part of the light curve, peaks at about 14 mag, and is non-relativistic at $t_\times$ with $\nu_{\rm m}^{\rm RS} < \nu_{\rm a}^{\rm RS} < \nu_{\rm R} < \nu_{\rm c}^{\rm RS}$. Therefore, $t_\times \approx 45$ s is greater than the prompt duration $T_{\rm dur} = (1+z)\frac{\Delta_0}{c} \approx 20$ s. The R band rising index is ~ 2.5, which is slower than the analytical estimation of NRS (Koboyashi 2000; Fan et al. 2002). It varies with time as well as with the initial parameters (Nakar & Piran 2004). After $t_\times$, the decay index is ~ 2 until $\nu_{\rm c}^{\rm RS} = \nu_{\rm R}$. Then a break occurs followed by a faster decay. The flux after the break comes from the equal arriving time surface emitted at the lower radius. Since $\nu_{\rm c}$ is reduced by SSC, it reaches the R band and the RS flux encounters a faster decay shortly after $t_\times$. Due to the rapid decay of the RS emission, the later emission is mainly contributed by the FS. It is interesting to note that the late FS emission bump vanishes when the SSC effect is taken into account. The physical reason is that with the SSC effect, the FS flux peak time appears earlier at $\nu_{\rm R} = \nu_{\rm c}^{\rm FS}$ during the fast cooling. Since $\nu_{\rm c}^{\rm FS} \propto t^{-1/2}$, $\nu_{\rm m}^{\rm FS} \propto t^{-3/2}$ and $F_{\rm max}^{\rm FS} \sim$ const., the decay index following the peak flux is quite flat (–1/4) and changes to $-(3p-2)/4$ after $\nu_{\rm R} = \nu_{\rm m}^{\rm FS}$.

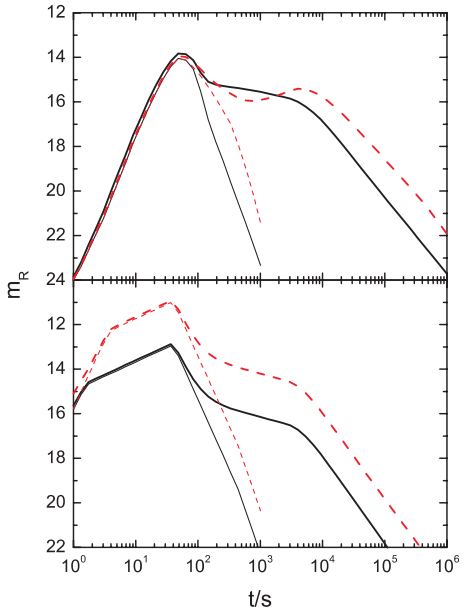

Fig. 2 R band afterglow from an isotropic ejecta with typical parameters. The upper panel shows the ISM case and the lower panel the wind case. Thin lines are the RS emission and thick lines are the total emission. The SSC effect is ignored in the dashed lines and is taken into account in the solid lines. In the ISM case, the shape of the light curve changed since $\nu_{\rm c}^{\rm RS}, \nu_{\rm c}^{\rm FS} \sim \nu_{\rm R}$ around $t_\times$. The RS shows a more rapid decay and the bump caused by the FS vanishes. In the wind case, both the RS and FS flux are reduced since $\max(\nu_{\rm c}^{\rm RS}, \nu_{\rm c}^{\rm FS}) < \nu_{\rm R}$. Parameters: $\eta = 300$, $\Delta_0 = 3 \times 10^{11}$ cm, $E_{\rm iso} = 1 \times 10^{53}$ erg, $n_1 = 1\,{\rm cm}^{-3}$ for ISM, and $\eta = 300$, $\Delta_0 = 1 \times 10^{12}$ cm, $E_{\rm iso} = 5 \times 10^{52}$ erg and $A_* = 1.0$ for wind, $\epsilon_{\rm e} = 0.3, \epsilon_{\rm B} = 0.01, p = 2.5$ and $z = 1$.

In the stellar wind environment, the RS also dominates the very early R band light curve with typical parameters: see the lower panel of Figure 2. The peak flux is about 13 mag. The RS is relativistic at $t_\times$ with $\nu_{\rm c}^{\rm RS} < \nu_{\rm a}^{\rm RS} < \nu_{\rm R} < \nu_{\rm m}^{\rm RS}$, and $t_\times \approx 40$ s coincides with $T_{\rm dur} \approx 65$ s. The R band rising index is ~ 0.5, which is much flatter than in the ISM case. After $t_\times$, the flux decays with –2.5, which is contributed by the emission from smaller radii in the equal arrival time surface. Since both the RS and FS are in the fast cooling case and $\max\{\nu_{\rm c}^{\rm RS}, \nu_{\rm c}^{\rm FS}\} < \nu_{\rm R}$, the R band flux is reduced by a factor of $1 + Y \simeq 1 + \sqrt{\epsilon_{\rm e}/\epsilon_{\rm B}}$ (about 2 magnitudes on taking $\epsilon_{\rm e}/\epsilon_{\rm B} = 30$) when the SSC effect is taken into account.

4.2 Uniform Jet

The Uniform jet is a simple model which assumes that all the ejected materials are confined to a collimated uniform cone. GRBs are detected within the cone (on-beam). XRFs and XRRGs are viewed out of the jet (off beam). If our viewing angle $\Theta_{\rm v}$ is slightly larger than the jet opening angle $\theta_{\rm jet}$, we will have the observed frequency

$$\nu_{\rm off} = a\nu_{\rm on}, \tag{19}$$

with $a \approx [1 + \gamma^2(\Delta\Theta)^2]^{-1}$ (γ is the bulk Lorentz factor of the jet) and $\Delta\Theta = \Theta_{\rm v} - \theta_{\rm jet}$. Taking the peak energy of XRFs, $E_{\rm p,XRF} \approx 0.1 E_{\rm p,GRB}$, XRFs should be observed at $\Delta\Theta_{\rm XRF} \approx 3/\eta$. The observed flux can be estimated by an empirical formula (e.g. Fan et al. 2004)

$$F_{\nu_{\rm off}}(\Delta\Theta, t_{\rm obs}) \approx \frac{a^3}{2} F_{\nu_{\rm on}}(0, t), \tag{20}$$

where ${\rm d}t_{\rm obs} = {\rm d}t/a$. It implies that if $\gamma > 1/\Delta\Theta$,the observed flux is dramatically lower and the observed time is longer. The early afterglow powered by the uniform jets is presented in Figure 3.

In the ISM case, the flux increases rapidly at the early time. The RS component reaches its peak flux at a time longer than viewing on-beam. The peak flux of the RS emission for $\Delta\Theta = 3/(2\eta)$ (i.e., the XRRG) is about 17.5 mag at about 100 s. It is bright enough to be detected. The rising index of RS is about 3.5 and the peak flux of the RS emission for $\Delta\Theta = 3/\eta$ (i.e., the XRF) is about 21 mag at about 250 s. Then it is hard to detect by *UVOT* on *Swift* or ground telescopes. The rising index is about 4.2. After $t_\times$ the observed FS flux continues to rise for a while, and peaks several hours later. The peak FS emission flux of the XRRG is about 17 mag and 17.5 mag for the XRF. Therefore, in XRFs the RS component can hardly be seen and the later FS component around 1 hour will be much brighter. In the XRRG the RS emission is detectable but will not be significant. The light curve is nearly flat for t <1 hour.

In the wind case, the off-beam RS very early flux increases at the same rate as in the on-beam case since both γ and a are constant, but the flux is lower. The peak time of the off-beam RS is slightly later, ~ 50 s for the XRF. The RS peak flux is about 15 mag and significantly brighter than the FS. After $t_\times$, as the Lorentz factor decreases the light curve gradually converges to the one from the center.

4.3 Nonuniform Jet

Different from uniform jets, there are emission materials on the line of sight in nonuniform jets (Gaussian or power-law). The XRFs and XRRGs are viewed within the jets but have lower isotropic-equivalent energy than GRBs. The observed early emission is mainly contributed by materials on the line of sight. However, we find that the light curve shows notable deviations when the RS is relativistic.

4.3.1 Gaussian Jet

The jet energy in a Gaussian jet with an angular distribution is

$$E(\theta) = E_0 e^{-\theta^2/2\theta_0^2}, \quad 0 \le \theta \le \theta_{\rm jet}. \tag{21}$$

For a typical value of $E_{\rm iso,XRF} = 10^{-2} E_{\rm iso,GRB}$, the viewing angle of the XRF should be $\Theta_{\rm v,XRF} \approx 3.04\theta_0$. We also calculate the light curve with $\Theta_{\rm v,XRRG} \approx 2.15\theta_0$, which may correspond to the XRRG (taking $E_{\rm iso,XRRG} = 10^{-1} E_{\rm iso,GRB}$). The R band afterglow from a Gaussian jet is shown in Figure 4.

In the ISM case, the off-axis RS flux is exactly the same as the isotropic emission taking $E_{\rm iso} = E(\Theta_{\rm v})$. The RS is non-relativistic and the Lorentz factor is high at early time. So the jet structure can not change the light curve significantly. As $\Theta_{\rm v}$ increases, $t_\times$ of the light curve gets earlier; and the peak RS emission flux gets lower, at about 17 mag for XRRG and 19.5 mag for XRF; (iii) the rise before $t_\times$ gets flatter; (iv) t_{Rc} (the time $\nu_{\rm R} = \nu_{\rm c}$) gets longer, hence a longer time interval for the ~ -2 delay after $t_\times$.

In the stellar wind case, the off-axis RS flux is slightly different from the isotropic emission $E_{\rm iso} = E(\Theta_{\rm v})$, the RS is relativistic and the Lorentz factor is sufficiently low as a reflection of the jet structure. The isotropic emission with decreasing $E_{\rm iso}$ from GRB to XRF has (i) nearly constant $t_\times$, a constant rising index 0.5 before $t_\times$ and a decay index -2.5 after $t_\times$; (ii) a lower peak flux, about 16.5 mag for the XRRG and 19 mag for the XRF. What the actual light curve differs from the isotropic one is the decay index of the RS flux. Viewing from the center, the RS flux decays faster. With increasing viewing angle, the start time of the faster decay increases, and from $t_\times$ to this time, the flux is flatter than the isotropic emission. The surplus emission comes from the center of the jet with $\theta < \Theta_{\rm v}$.

4.3.2 Power-law Jet

In this model, the jet energy as a function of the viewing angle is

$$E(\theta) = \begin{cases} E_c\,, & 0 \le \theta < \theta_c, \\ E_c(\theta/\theta_c)^{-2}\,, & \theta_c \le \theta \le \theta_{\rm jet}. \end{cases} \tag{22}$$

$E_{\rm iso,XRF} = 10^{-2} E_{\rm iso,GRB}$ and $E_{\rm iso,XRRG} = 10^{-1} E_{\rm iso,GRB}$ correspond to $\Theta_{\rm v,XRF} \approx 10\theta_c$ and $\Theta_{\rm v,XRRG} \approx 3.16\theta_c$, respectively. The early afterglow from a power-law jet is shown in Figure 5.

In the ISM case, the RS is also exactly the same as the isotropic emission with $E_{\rm iso} = E(\Theta_{\rm v})$, as found in the Gaussian jet model. In the wind case, the RS flux also resembles that in the Gaussian jet except the decay index departs more from the isotropic emission.

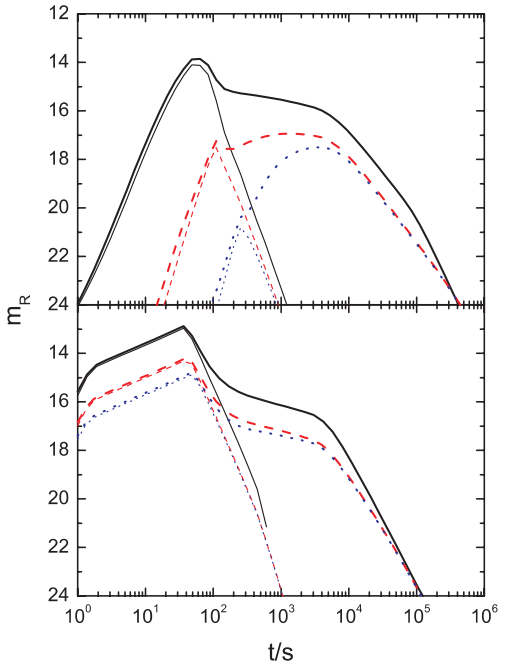

Fig. 3 R band afterglow from a uniform jet. Upper panel shows the ISM case and the lower panel the wind case. Thin lines are the RS emission and thick lines are the total emission. $\Delta\Theta = 0,\ 3/2\eta,\ 3/\eta$ for the solid, dashed and dotted lines, respectively. Parameters: $\theta_{\rm jet} = 0.1$, other parameters are the same as in Fig. 2.

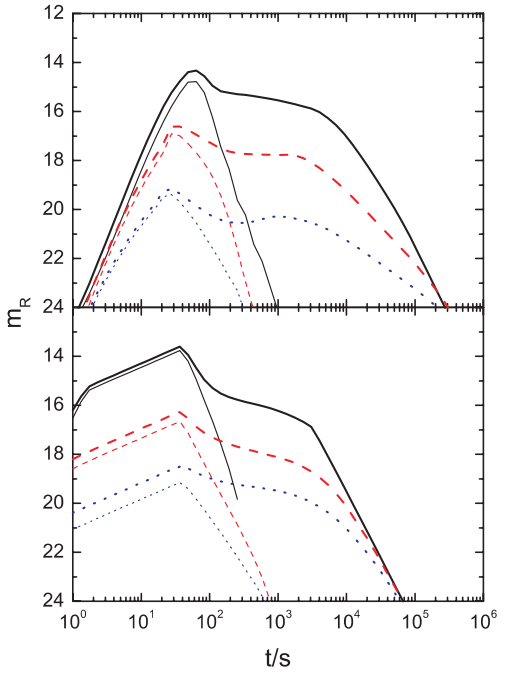

Fig. 4 R band afterglow from a Gaussian jet. The upper panel shows the ISM case and lower panel the wind case. Thin lines are the RS emission and thick lines are the total emission. We take $\Theta_{\rm v} = 0, 2.15\theta_0, 3.04\theta_0$ in the solid lines, dashed lines and dotted lines, respectively. Parameters: $E_0 = 1\times10^{53}$ erg for ISM and $E_0 = 5\times10^{52}$ erg for wind, $\theta_0 = 0.05$, $\theta_{\rm jet} = 0.2$, other parameters are the same as in Fig. 2.

5 CONCLUSIONS AND DISCUSSION

So far, there are several RS emission candidates reported in *Swift* era, including GRB 041219a, GRB 050904, GRB 060111b, and possibly GRB 050525a. It is very interesting to note that all these reverse shock regions are likely to be mildly magnetized (Fan et al. 2005b; Wei et al. 2006).

However, among all the bursts targeted in optical band within few minutes after the prompt emission, most have no RS emission component (e.g., Ronning et al. 2006). The physical reason is so far not clear. One speculation is that the GRB/XRF/XRRG outflow is Poynting-flux dominated, even after the prompt $\gamma-$ray emission phase (Zhang & Kobayashi 2005; Fan et al. 2004b). However, we still need direct evidence for such a model. Recently Molinari et al. (2007) reported the non-detection of infrared RS component in GRB 060418 and GRB 060609A. Jin & Fan (2007) attributed the weak reverse shock emission in these two bursts to a very small $\nu_{\rm m}^{\rm RS}$. They also argued that this interpretation could account for the weak reverse shock emission in a group of *Swift* GRBs. One may also think the extinctions of the host galaxy plays an important role. Here we do not go further and just outline the lack of bright optical flashes in GRBs/XRFs/XRRGs as a major puzzle among the community.

In this paper, we numerically calculated the early afterglow powered by various kinds of jets. The dynamical evolution is solved from a set of differential equations. This is different from the analytical treatment of Fan et al. (2004a) and gives similar but more exact results. We find that the most of the uncertainty of estimation comes from $\gamma_{34} - 1$, which results in the overestimation of $\nu_{\rm m}$ and a too rapid increase of $\nu_{\rm m}$ before $t_\times$ in the previous treatment. This is especially significant in the ISM case since, there, the RS is mildly relativistic for the typical parameters taken here. At the same time, $\nu_{\rm c}$ was overestimated previously

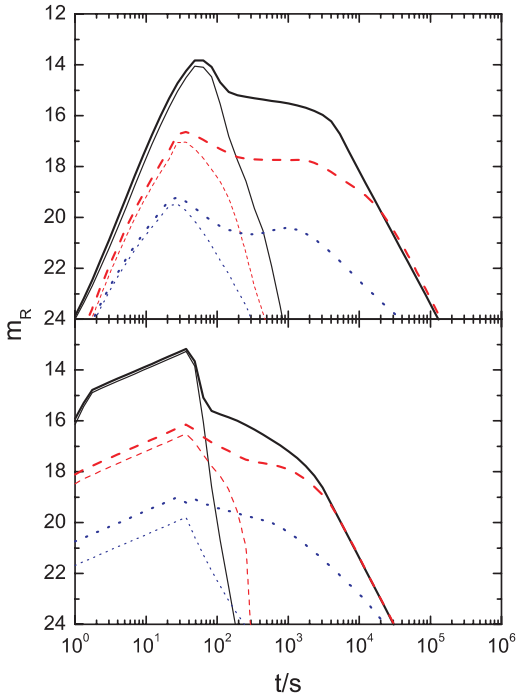

Fig. 5 R band afterglow from a power-law jet. The upper panel shows the ISM case and the lower panel the wind case. Thin lines are the RS emission and thick lines the total emission. $\Theta_{\rm v} = 0, 3.16\theta_c, 10\theta_c$ in the thick lines, dashed lines and dotted lines, respectively. Parameters: $E_c = 1 \times 10^{53}$ erg for ISM and $E_c = 5 \times 10^{52}$ erg for wind, $\theta_c = 0.015$, $\theta_{\rm jet} = 0.2$, other parameters are the same as in Fig. 2.

because of ignoring the SSC effect. Considering these two factors, the peak flux of the reverse shock should be lower, which may help us to explain the lack of detection of optical flashes in most GRBs. It also needs to point out that electrons may be cooled not only by the SSC process but also by the external photons(e.g., prompt emission) through inverse Compton scattering. Then $\nu_{\rm c}$ may reduce further and lead to even fainter very early optical radiation.

We calculated the early afterglow from both uniform and structured jets. We find that the early afterglow varies significantly with different viewing angles and is dependent on the jet structure.

Swift XRT detection has revealed that early X-ray flare may be a common characteristic of GRB X-ray afterglow. Fan & Wei (2005) and Zhang et al. (2006) suggested that the RS synchrotron emission can hardly produce very early X-ray flares. Our calculation confirms their results. We also tried to simulate it with RS SSC emission within a large parameters space, but failed. The RS SSC X-ray emission is always lower and generally far lower than the FS synchrotron emission.

Acknowledgements We thank Zou, Y. C. and Jin, Z. P. for helpful discussions. This work is supported by the National Natural Science Foundation of China (NSFC, Grants 10225314 and 10233010), and the National 973 Project on Fundamental Researches (NKBRSF G19990754).

References

Akerlof C. W., Balsano R., Barthelmy S. et al., 1999, Nature, 398, 400
Barraud C., Olive J.-F., Lestrade J. P. et al., 2003, A&A, 400, 1021
Blake C. H., Bloom J. S., Starr D. L. et al., 2005, Nature, 435, 181
Blandford R. D., Mckee C. F., 1976, Phys. Fluids, 19, 1130
Boër M., Atteia J. L., Damerdji Y. et al., 2006, ApJ, 638, L71
Chevalier R. A., Li Z. Y., 2000, ApJ, 536, 195
Costa E., Frontera F., Heise J. et al., 1997, Nature, 387, 783
Dai Z. G., Lu T., 1998, MNRAS, 298, 87
Dai Z. G., Lu T., 2001, ApJ, 551, 249
Dermer C. D., Chiang J., Böttcher M., 1999, ApJ, 513, 656
Fan Y. Z., Dai Z. G., Huang Y. F., Lu T., 2002, Chin. J. Astron. Astrophys. (ChJAA), 2, 449
Fan Y. Z., Wei D. M., 2005, MNRAS, 364, L42
Fan Y. Z., Wei D. M., Wang C. F., 2004a, MNRAS, 351, L78
Fan Y. Z., Wei D. M., Wang C. F., 2004b, A&A, 424, 477
Fan Y. Z., Zhang B., Wei D. M., 2005a, ApJ, 628, 298
Fan Y. Z., Zhang B., Wei D. M., 2005b, ApJ, 628, L25
Fox D. W., Price P. A., Soderberg A. M. et al., 2003, ApJ, 586, L5
Heise J., in't Zand J., Kippen R. M., Woods P. M., 2001, In: Proc. of the Conference "Gamma-ray Bursts in the Afterglow Era", p.16
Huang Y. F., Dai Z. G., Lu T., 2002, MNRAS, 332, 735
Huang Y. F., Gou L. J., Dai Z. G., Lu T., 2000, ApJ, 543, 90
Ioka K., Nakamura T., 2001, ApJ, 554, L163
Jin Z. P., Fan Y. Z., 2007, MNRAS, 378, 1043
Jin Z. P., Wei D. M., 2004, Chin. J. Astron. Astrophys. (ChJAA), 4, 473
Klotz A., Boer M., Atteia J. L. et al., 2005, A&A, 439, L35
Klotz A., Gendre B., Stratta G. et al., 2006, A&A, 451, L39
Koboyashi S., 2000, ApJ, 545, 807
Koboyashi S., Sari R., 2000, ApJ, 542, 819
Koboyashi S., Zhang B., 2003, ApJ, 597, 455
Kumar P., Panaitescu A., 2003, MNRAS, 346, 905
Kumar P., Granot J., 2003, ApJ, 591, 1075
Kulkarni S. R., 1999, ApJ, 522, L97
Lamb D. Q., Donaghy T. Q., Graziani C., 2005, ApJ, 620, L355
Li Z., Dai Z. G., Lu T., Song L. M., 2003, ApJ, 599, 380
Li W., Filippenko A. V., Chornock R., Jha S., 2003, ApJ, 586, L9
Lloyd-Ronning N. M., Dai X. Y., Zhang B., 2004, ApJ, 601, 371
Mangano V., La Parola V., Cusumano G. et al., 2007, ApJ, 654, 403
McMahon E., Kumar P., Piran T., 2006, MNRAS, 366, 575
Mészáros P., Rees M. J., 1997, ApJ, 476, 332
Mészáros P., Rees M. J., Wijers R. A. M. J., 1998, ApJ, 499, 301
Mészáros P., Rees M. J., 1999, MNRAS, 306, L39
Molinari E., Vergani S. D., Malesani D. et al., 2007, A&A, 469, L13
Nakar E., Piran T., 2004, MNRAS, 353, 647
Panaitescu A., Kumar P., 2004, MNRAS, 353, 511
Roming, P. W. A., Schady P., Fox, D. B. et al., 2006 , ApJ, 652, 1416
Romano P., Moretti A., Banat P. L. et al., 2006, A&A, 450, 59
Rybicki G. B., Lightman A. P., 1979, Radiative Processes in Astrophysics, New York: Wiley
Sari R., Piran T., Narayan R., 1998, ApJ, 497, L17
Sari R., Piran T., 1995, ApJ, 455, L143
Sari R., Piran T., 1999, ApJ, 517, L109
Sari R., Esin A. A., 2001, ApJ, 548, 787
Shao L., Dai Z. G., 2005, ApJ, 633, 1027

van Paradijs J., Groot P. J., Galama T. et al., 1997, Nature, 386, 686
Wang X. Y., Dai Z. G., Lu T., 2001, ApJ, 546, L33
Wei D. M., 2003, A&A, 402, L9
Wei D. M., Lu T., 1998, ApJ, 505, 252
Wei D. M., Yan T., Fan Y. Z., 2006, ApJ, 636, L69
Wijers R. A. M. J., Galama T. J., 1999, ApJ, 523, 177
Wu X. F., Dai Z. G., Huang Y. F., Lu T., 2003, MNRAS, 342, 1131
Yamazaki R., Ioka K., Nakamura T., 2002, ApJ, 572, L31
Zhang B., 2007, Chin. J. Astron. Astrophys. (ChJAA), 7, 1
Zhang B., Fan Y. Z., Dyks J. et al., 2006, ApJ, 642, 354
Zhang B., Kobayashi S., 2005, ApJ, 628, 315
Zhang B., Mészáros P., 2002, ApJ, 571, 876
Zhang B., Kobayashi S., Mészáros P., 2003, ApJ, 595, 950
Zhang B., Dai X. Y., Lloyd-Ronning N. M., Mészáros P., 2004, ApJ, 601, L119
Zou Y. C., Wu X. F., Dai Z. G., 2005, MNRAS, 363, 93